Published in final edited form as:
*J Comp Neurol*. 2009 December 10; 517(5): 633–644. doi:10.1002/cne.22176.

# Differential Role for Synaptojanin 1 in Rod and Cone Photoreceptors

**LARS C. HOLZHAUSEN**, **ALARON A. LEWIS**, **KIMBERLY K. CHEONG**, and **SUSAN E. BROCKERHOFF***
University of Washington, Department of Biochemistry, Seattle, Washington 98195

## Abstract

Synaptojanin 1 (SynJ1) is a polyphosphoinositide phosphatase involved in clathrin-mediated endocytosis in conventional synapses. Studies with the zebrafish mutant *nrc* have revealed that loss of SynJ1 also affects cone photoreceptor ribbon synapses, causing pronounced morphological and functional abnormalities. In this study we continue to examine the role of SynJ1 in photoreceptors. Using a newly generated antibody specific for zebrafish SynJ1, we localized this protein predominantly to cone photoreceptors. We then used blastula stage transplantation experiments to demonstrate that rods from *nrc* mutants lacking SynJ1 develop normally and do not have the pronounced morphological defects detected in cones. Given the known involvement of SynJ1 in synaptic vesicle endocytosis, we hypothesize that rods and cones use distinct mechanisms for vesicle recycling.

### Indexing terms

synaptojanin; zebrafish; photoreceptors; ribbon synapse; endocytosis

Distinction in the physiological properties of rod and cone photoreceptors is a key feature of human visual abilities. Rods are responsible for night and low-light vision, are more sensitive to light, and respond more slowly than cones. Cones have a much faster light response, a higher stimulation threshold, and are responsible for daytime and color vision (Korenbrot and Rebrik, 2002; Fu and Yau, 2007; Kawamura and Tachibanaki, 2008). These differences in response kinetics of rods and cones were observed in the original measurements of light-induced electrical responses of photoreceptors. We now know that these properties in phototransduction kinetics are conveyed to downstream cells by unique synaptic transmission within these two cell classes. For example, studies in salamander indicate that the initial fast component of exocytosis has a time constant of <5 ms in cones, >10-fold faster than that of rods (Thoreson, 2007).

Despite a clear description of the many physiological differences between rod and cone photoreceptors, the molecular explanation for these distinctions is unclear. Phototransduction and synaptic transmission in rods and cones depends on similar molecular cascades using analogous basic mechanisms (Chen, 2005). The two cell classes use different isozymes, splice variants, and homologs of the same proteins to produce light-dependent signaling. These shared features suggest that most of the physiological differences will be



*Correspondence to: Susan E. Brockerhoff, University of Washington, Department of Biochemistry, Box 357350, Seattle WA, 98195., sbrocker@u.washington.edu.

Additional Supporting Information may be found in the online version of this article.

explained by the sum of many small regulatory and enzymatic differences. However, there are many aspects of signaling that have yet to be explored for which there may be completely different molecular mechanisms in each cell class. In support of this latter idea, a retinoid cycle was recently identified that is used exclusively by cone photoreceptors to regenerate cone opsin (Arshavsky, 2002; Mata et al., 2002, 2005).

In zebrafish, cone photoreceptors mature significantly more rapidly than rods (Branchek, 1984). Thus, young zebrafish larvae primarily use cones for vision. This protracted developmental timeline has provided an effective strategy for dissecting pathways unique to cone photoreceptors. Mutagenesis screens analyzing the visual behavior of larvae identify genes disrupting exclusively cone function or both rod and cone function (Brockerhoff et al., 2003; Muto et al., 2005; Taylor et al., 2005; Stearns et al., 2007). Genes selective to rods are not found using this strategy. Additionally, since behavioral screening approaches are unbiased, genes essential for many aspects of cone function such as phototransduction, synaptic transmission, and protein transport are being uncovered (Brockerhoff et al., 2003; Van Epps et al., 2004; Muto et al., 2005; Taylor et al., 2005; Stearns et al., 2007).

One mutant, *nrc*, identified by visual behavioral screening in zebrafish, has abnormal visual responses caused by dramatic abnormalities in the morphology of the cone synapse including floating ribbons, aggregated clusters of synaptic vesicles, reduced vesicle number, and a lack of horizontal and bipolar invaginations into the pedicle (Allwardt et al., 2001; Van Epps et al., 2001). This phenotype is due to a null mutation in the polyphosphoinositide phosphatase, Synaptojanin 1 (SynJ1) (Van Epps et al., 2004). SynJ1 is a widely expressed presynaptic protein, which is critical at many synapses, although its importance for the photoreceptor had not been previously demonstrated. In conventional synapses the loss of SynJ1 causes a dramatic accumulation of clathrin-coated synaptic vesicles leading to the hypothesis that dephosphorylation of $PIP_2$ facilitates clathrin uncoating (Cremona et al., 1999; Harris et al., 2000). Interestingly, electron microscopy (EM) analysis did not find increased numbers of clathrin-coated vesicles at the *nrc* mutant cone pedicle (Van Epps et al., 2004). These findings suggest a dramatic and potentially unique role for polyphosphoinositides at cone pedicles.

In this study we set out to gain a clearer understanding of SynJ1 function in photoreceptors. Loss of SynJ1 is lethal and *nrc* mutants die prior to developing significant numbers of mature rod photoreceptors. Thus, as a first step we generated an antibody specific to zebrafish SynJ1 to determine in wild-type (WT) zebrafish whether this phosphatase is expressed exclusively in cones or in both rod and cone photoreceptors. Further, we evaluated whether rod photoreceptors from the *nrc* mutant lacked invaginated synapses similar to cones. To do this, we conducted a mosaic analysis in which rod photo-receptors from the SynJ1 mutant *nrc* were transferred into WT host embryos. Using these strategies we report that SynJ1 is necessary for normal cone but not rod synapse formation. SynJ1 protein concentrates in cone synapses and accordingly the morphology of rod spherules from SynJ1 null fish is normal. We propose that SynJ1 defines a molecular pathway that is unique to cone photoreceptors and that deciphering the function of this protein in cones will help explain some of the unique physiological properties of rods versus cones.

## MATERIALS AND METHODS

### Zebrafish maintenance and optokinetic response (OKR) screening

Zebrafish stocks are maintained in the University of Washington Zebrafish Facility. Adult and larval fish are grown at 28.5°C in reverse-osmosis distilled water reconstituted for fish compatibility by addition of salts and vitamins (Westerfield, 1995) on a 10/14-hour dark/

light cycle. The OKR visual behavioral screening of *nrc* mutants was done as described (Brockerhoff, 2006).

## Cloning and protein expression

The full-length zebrafish *synJ1* gene (*NP_001007031*) was cloned into pTriEx-4 vector (Novagen, Madison, WI) so that the His-tag encoded by the vector was attached to the C-terminal end of the gene. This construct was used to transfect Human Embryonic Kidney-293 (Hek-293) cells maintained at 37°C in Dulbecco's Modified Eagle Medium (D-MEM, Gibco, Grand Island, NY) supplemented with 10% fetal bovine serum (Gibco) and 100 $\mu$g/mL of a penicillin-streptomycin solution (Sigma, St. Louis, MO). Cells were transfected using Fugene transfection reagent (Roche, Nutley, NJ) following the manufacturer's recommendations. Transfected cells were harvested after 48 hours in the incubator.

## Harvesting of cells and protein purification

Hek-293 cells were harvested by first detaching them from the plates with 1 mL of a 0.25% Trypsin-EDTA solution (Gibco). Cells were then resuspended with 5 mL of D-MEM. This mixture was transferred to Falcon tubes and centrifuged for 5 minutes at 500*g* at 4°C. Cell pellets were washed once with phosphate-buffered saline (PBS, pH 7.4), recentrifuged and stored at −80°C until purification. Protein was purified using a His-tag Ni-column chromatography kit from Novagen following the manufacturer's recommended protocol. Briefly, cells were thawed on ice and lysed with 1 mL of mammalian protein extraction reagent (M-PER, Pierce, Rockford, IL) per 100 $\mu$L of cell pellet. This suspension was rotated for 10 minutes at 4°C, and then spun for 10 minutes at 16,000*g* at 4°C. The supernatant was applied to the washed and "charged" resin. After 1 hour incubation in Eppendorf tubes at 4°C, the resin-lysate solution was applied to a G-50 column and drained by gravity flow. After elution the protein was dialyzed against 1 × PBS overnight at 4°C. Purified protein was stored at −20°C.

## Antibody characterization

All antibodies used in this study are listed in Table 1.

**Anti-SynJ1 antibody—**Full-length His-tagged zebrafish SynJ1 protein was used to generate a monoclonal antibody that specifically recognizes SynJ1 (Fig. 1). SynJ1 antibody was collected as supernatant from antibody producing monoclonal hybridoma cell cultures. Antibody production was done using the NIH-sponsored UW Vision Core Facility (EY01730). The SynJ1 antibody was characterized by immunoblotting with brain tissue and by immunohistochemistry (IHC) with retinal tissue. The specificity was confirmed using tissue from SynJ1 null *nrc* mutant zebrafish (see Results and Fig. 1).

**Anti-mGluR5 antibody—**The mGluR5 antibody AB5675 (Table 1) was used to label cone pedicles. According to the manufacturer's data sheet (http://www.millipore.com/catalogue/item/ab5675), this antibody stains a single band of 132 kD on Western blots of rat brain microsomes. Previous work in zebrafish (Yazulla and Studholme, 2001) has shown that this antibody stains a retinal pattern consistent with it identifying cone pedicles. We verified that the cone pedicles were selectively labeled with this mGluR5 antibody by using transgenic zebrafish, *Tg(TalphaC:EGFP)*, that express enhanced green fluorescent protein (EGFP) under the control of the zebrafish cone transducin promoter (Suppl. Fig. 1). Finally, the retinal staining pattern we observed using AB5675 is similar to a well-characterized different mGluR5 antibody, Chemicon

(Temecula, CA) antibody 06–451, previously used on the goldfish retina (Joselevitch et al., 2007).

**Anti-His-Tag antibody—**The His-tag antibody was used to follow the purification of full-length His-tagged Synaptojanin 1 from Hek-293 cells. This antibody was not used to localize Synaptojanin 1 in zebrafish.

## Protein expression, Western blots

Sodium dodecyl sulfate-polyacrylamide gel electrophoresis (SDS-PAGE) (BioRad, Hercules, CA; 4%–20% gradient gels), Western blot analysis, and silver staining (Amersham, Arlington Heights, IL) were used to evaluate SynJ1 expression/purification. For Westerns, the primary antibody, mouse-$\alpha$-His-tag antibody (Invitrogen, La Jolla, CA), was diluted 1:1,000 and the secondary antibody, $\alpha$-mouse-HRP linked antibody from goat (Amersham), was diluted 1:4,000. Results were analyzed with ECL chemiluminescent reagents (Amersham) according to the manufacturer's instructions. To assess the specificity of the generated monoclonal antibody by Western blot analysis, we prepared Hek-293 cell lysates that were transfected with SynJ1 by boiling harvested Hek-293 cells in 1 × SDS sample buffer. Brain samples for Western blot analysis were prepared as described previously (Van Epps et al., 2004). All samples were treated with benzonase (Roche Applied Sciences) before loading on SDS-PAGE. After transfer onto nitrocellulose membranes (Millipore, Bedford, MA), membranes were blocked in Odyssey blocking buffer (LI-COR Biosciences, Lincoln, NE). Membranes were incubated overnight at 4°C with monoclonal anti-zfSynJ1 (diluted 1:5 in blocking buffer). Primary antibody was detected with IRDye-800CW goat antimouse secondary antibody (LI-COR Biosciences) and fluorescent signals were detected with the Odyssey Infrared Imaging System (LI-COR Biosciences).

## IHC

The antibody works effectively in IHC undiluted, with ON incubation at 4°C. IHC on 20-$\mu$m sections was done as described previously (Brockerhoff et al., 1997). For the double-label of cone synapses the rabbit anti-mGluR5 (AB5675, Chemicon) was used as previously described (Yazulla and Studholme, 2001). Secondary antibodies were coupled to Alexa 488, 568, and 633 (Molecular Probes, Eugene, OR). Propidium iodide (Molecular Probes) was used as nuclear stain. All secondary antibodies and nuclear stains were used according to the manufacturer's recommendations. The specificity of the primary antibody staining in IHC was evaluated by processing sections in the absence of these antibodies. No immunostaining was detected with secondary antibodies alone.

## Transgenic zebrafish

Transgenic fish strains used were *Tg(xops:EGFP),* expressing EGFP in rods under the control of the *Xenopus* opsin promoter (Fadool, 2003), *Tg(nyx:MYFP)* expressing membrane-tagged YFP in a subset of ON-type bipolar cells under the control of the nyctalopin promoter (Schroeter et al., 2006), *Tg(TalphaC:EGFP)* expressing EGFP under the control of the cone alpha transducin promoter (Kennedy et al., 2007) and *Tg(TalphaC:spH)* expressing synapto-pHluorin (Miesen-bock et al., 1998) under the control of the cone alpha transducin promoter (Kennedy et al., 2007). To express synapto-pHluorin in zebrafish cones we subcloned 3.2 kb of the cone alpha transducin promoter (Kennedy et al., 2007), the modified Gal4-Vp16 binding protein (Koster and Fraser, 2001), 5 UAS sequence motifs (Brand et al., 1994) and the full-length ecliptic synapto-pHluorin gene (Miesenbock et al., 1998) into the modified tol2 vector (Taylor et al., 2005). The resulting

construct was injected into WT zebrafish larvae together with tol2 transposase mRNA as previously described (Taylor et al., 2005).

## Imaging

For microscopic analysis we recorded image stacks of labeled retinal sections with conventional widefield or confocal microscopy. For widefield microscopy, sections were examined with the Nikon E1000 widefield epifluorescence microscope using a 40 × 1.3 NA oil immersion objective (Zeiss). Image stacks were obtained as single optical slices (0.18 $\mu$m) and subsequently deconvolved using the Scientific Volume Imaging's Huygens Essential deconvolution software. For confocal microscopy, sections were viewed with either the laser scanning microscope LSM510 (Zeiss, Thornwood, NY) using an inverted 40×, 1.3 NA oil immersion objective (Zeiss), or the Olympus FluoView-300 using a 60×, 1.42 NA oil immersion objective (Zeiss), or the Olympus FluoView-1000 using a 60×, 1.42 NA oil immersion objective (Zeiss). Image stacks were recorded as single optical slices (0.18 – 0.3 $\mu$m). Recorded image stacks were normalized and projected into single images with NIH Image J. Image contrast and brightness was adjusted using Adobe Photoshop v. CS3 (San Jose, CA).

**Fluorescence signal intensity profiles—**For the fluorescence signal intensity profiles, we first selected the outer plexiform layer (OPL) as a region of interest (ROI) and de-marked this region with a rectangle. We chose the ROI so that only fluorescent signals from synapses would be included for the analysis, but not signal from other sources such as cell bodies or background. We then used NIH Image J to plot the intensity profile for the ROI across the OPL. Intensities within the ROI were averaged across the vertical direction to give a single average intensity for each horizontal position. Horizontal position across the OPL represents the x-axis in Figures 3 and 4. Finally, we corrected for background fluorescence by subtracting the average background level from an area outside of the ROI, and we normalized data to compensate for differences in overall fluorescent signal strength. The intensity profiles shown are from a single optical slice. The intensity profiles correlate to the presented image data for all except Figure 3F, where the intensity signal from the final synapse on the right is not shown.

## Blastula stage transplantations

Blastula stage transplantations were done as described (Carmany-Rampey and Moens, 2006). We crossed the *nrc* mutation, *nrc*$^{a14}$ (Van Epps et al., 2004) with *Tg(xops:EGFP)* (Fadool, 2003), *Tg(TalphaC:EGFP*) (Kennedy et al., 2007), and *Tg(TalphaC:spH)* zebrafish. Embryos from crosses between fluorescent-positive adults heterozygous for the *nrc* allele were used as donors in our experiments. The hosts were WT embryos. This strategy resulted in *nrc* to WT, heterozygote to WT, and finally WT to WT transplants. All donors were genotyped for the *nrc* allele and screened for an OKR response. Since WT and *nrc* heterozygotes appear indistinguishable, we refer to all OKR-positive donors as WT. All mutant donors lacked an OKR response. For the *nrc* genotyping we amplified a polymerase chain reaction (PCR) product with primers Int11.F2 (TCCTTTGAATACATGTGCATGAG) and Ex11.R5 (CATATAGGCTGCTTGTCGTG) that spans Exon11 with the *nrc* mutation and part of the preceding intron. This PCR product was then sequenced (primer: CACCAGAACCATCCA-GAACA) to verify the presence of the *nrc* mutation (Van Epps et al., 2004). Hosts that contained fluorescent-positive cells within the retina at 4 days postfertilization (dpf) were further grown for ≈ 16 dpf to allow rods to develop and mature or 5–6 dpf to analyze cones. Retinas were then fixed, embedded in OCT, sectioned at 20 $\mu$m, and fluorescent-positive rod spherules or cone pedicles were analyzed using confocal microscopy.

# RESULTS

## Synaptojanin 1 protein purification and antibody specificity

Full-length zebrafish (zf) Synaptojanin 1 (SynJ1) protein was expressed in Hek-293 cells, purified, and used to generate a monoclonal antibody (see Materials and Methods and Fig. 1A). Immunoblotting experiments using brain extracts from WT zebrafish larvae and adults identified a single protein at ≈ 150 kDa. This protein was absent in SynJ1 null (*nrc*) brain extracts (Fig. 1B). This result agrees with the reported size of native SynJ1 (McPherson et al., 1994) and was further confirmed by immunoblots with recombinant zfSynJ1 overexpressed in tissue culture, which also showed a major protein band at this size (Fig. 1B). The absence of the 150-kDa protein band in brain extracts from mutant zebrafish *nrc* larvae demonstrated the specificity of this monoclonal antibody for SynJ1.

As further confirmation of antibody specificity, we labeled the retinas of WT (SynJ1-positive) zebrafish larvae and SynJ1 null *nrc* mutant larvae and compared the labeling (Fig. 1C,D). Although clear staining of both the OPL and inner plexiform layer (IPL) was evident in the WT retina, this staining was absent from the *nrc* mutant retina. This indicates that the antibody specifically recognizes SynJ1 in IHC experiments.

## Synaptojanin 1 is predominantly presynaptic in the OPL and is present in photoreceptor inner segments

Previous studies localized SynJ1 to both the OPL and IPL of the zebrafish retina (Van Epps et al., 2004). However, a detailed analysis of SynJ1 localization within the retina has not been reported. Since SynJ1 is critical for cone pedicle morphology and function, we analyzed SynJ1 distribution in photoreceptors. Figure 2A–D shows that the immunostaining for SynJ1 in the OPL is primarily localized to the presynaptic region within photoreceptor terminals. We used a transgenic fish strain expressing YFP in a subset of bipolar cells in order to define postsynaptic invaginations into the photoreceptor terminal. We found that OPL staining correlated strongly with the region of the photoreceptor terminal not containing postsynaptic dendrites, although it is difficult to rule out the possibility that the bipolar dendrites do express low levels of SynJ1 (Fig. 2B). This finding agrees with previous work indicating that SynJ1 localization is predominantly presynaptic (McPherson et al., 1996).

Additionally, we found that the inner segment of cone photoreceptors contained SynJ1 protein. The inner segment contains the mitochondria and is located directly under the outer segment. Clear immunoreactivity was detected in this region of cone photoreceptors within the adult and larval retina. Figure 2E shows an adult section and 2F shows a larval section at high magnification. The shape and position of the outer segment in SynJ1-positive cells in the light-adapted retina indicates that these are cone photoreceptors. One possible explanation for this finding is that SynJ1 accumulates at its site of synthesis. However, another possibility is that SynJ1 has additional roles in photoreceptor biology that extend beyond synapse function and morphology. In yeast, synaptojanin-like proteins function in post-Golgi vesicle transport (Bensen et al., 2000). Consistent with this latter hypothesis, we find that the *nrc* mutants expressing the transgene *Tg(TalphaC:spH)* have increased membrane fluorescence in their inner segment compared to WT, suggesting a possible accumulation of vesicles in this region (Fig. 5).

## Synaptojanin 1 is concentrated in cone pedicles

Previous characterization of the *nrc* mutant (Van Epps et al., 2004) and the initial SynJ1 antibody staining suggested that SynJ1 is localized in cones, but it was less clear whether rods also contained SynJ1. To determine whether SynJ1 primarily localized to both cones

and rods or only cones, we conducted colocalization experiments. We colabeled retinal sections with the zfSynJ1 antibody and the rat metabotropic glutamate receptor 5 (mGluR5) antibody, which was previously characterized as specifically labeling zebrafish cones (Yazulla and Studholme, 2001; Suppl. Fig. 1). Additionally, we stained retinas from the cone-specific transgenic line *Tg(TalphaC:EGFP)* and the rod-specific transgenic line *Tg(xops:EGFP)*, expressing EGFP in cones or rods, respectively, with the zfSynJ1 antibody to visualize colocalization with these cell-type-specific fluorescent proteins (Figs. 3, 4).

Figure 3 shows colocalization experiments using anti-zfSynJ1 antibody and the transgenic line *Tg(TalphaC:EGFP)* (Fig. 3A–C) or a polyclonal antibody against the mGluR5 (Fig. 3E–H). The transgenic zebrafish line *Tg(TalphaC:EGFP)* directs EGFP expression specifically to cones using the cone transducin promoter (Kennedy et al., 2007) and uniformly labels cone cell bodies and synapses (Kennedy et al., 2007; and Fig. 3C). Retinal sections from this fish strain that were immunolabeled with anti-zfSynJ1 reveal punctate SynJ1 expression in the OPL that colocalizes with the EGFP-containing cone pedicles and resembles the shape of cone pedicles (Fig. 3A–C). Similarly, we find that SynJ1 colocalizes with mGluR5 and labels cone synapses (Fig. 3E–H). In order to verify this observation, we plotted and overlaid the single-optical slice signal intensity profiles within the OPL for anti-zfSynJ1 and *TalphaC:EGFP* (Fig. 3D) or mGluR5, respectively (Fig. 3I). We found for both that the peaks and valleys of signal intensity correlated between zfSynJ1-immunoreactivity and these cone-specific markers.

During the colocalization experiments with cone-specific markers, we noticed a reduction of anti-zfSynJ1 signal between cones, indicating a possible lack of SynJ1 labeling in the rod terminals. To determine whether rods were indeed less intensely labeled by the anti-zfSynJ1 antibody, we then labeled sections obtained from the retina of the transgenic fish line *Tg(xops:EGFP)*. This transgenic fish strain contains EGFP under the control of the *Xenopus* opsin promoter, which directs EGFP expression exclusively in rod photoreceptors within the retina (Fadool, 2003). Staining of these transgenic sections with anti-zfSynJ1 showed little overlap between EGFP in rod photoreceptors and SynJ1 (Fig. 4A–E). Notably, the intensity profiles for anti-zfSynJ1 and *xops:EGFP* do not show signal correlation, suggesting the absence or reduction of SynJ1 in rod terminals (Fig. 4F). We also conducted a triple-label experiment in which rod terminals were labeled with *Tg(xops:EGFP)*, cone pedicles were labeled with mGluR5, and the retina was stained with anti-zfSynJ1 (Fig. 4G–J). As expected, there was no colabeling of *xops:EGFP* with the mGluR5 immunostaining. Furthermore, the immunolabel of SynJ1 predominantly colocalizes with mGluR5, and not with EGFP-labeled rod terminals (colocalized SynJ1 and mGluR5 labels appear magenta in the merged image, Fig. 4G). The intensity profiles of *xops:EGFP*, anti-SynJ1, and mGluR5 confirm that anti-zfSynJ1 and mGluR5 positively correlate with each other, but not with the profile of *xops:EGFP* (Fig. 4K).

Together these data indicate that SynJ1 is abundant in cone but not in rod photoreceptor terminals.

## Rod photoreceptor synapses appear normal in the absence of SynJ1

Our data indicate that SynJ1 is predominant in cone, but not rod photoreceptors. This implicates a unique requirement in cone photoreceptors for polyphosphoinositide metabolism. To verify this, we specifically examined rod synapse morphology from fish lacking SynJ1. In the *nrc* mutant, cone synapses are flat (not invaginated) and ribbons float within the cytoplasm and are not anchored to the membrane (Van Epps et al., 2004). We wondered whether *nrc* rods would similarly lack invaginated synapses. If rods do not require SynJ1 for normal function, *nrc* rods should have a WT morphology. This analysis had not been done in the original study analyzing SynJ1 null zebrafish because rod spherules

develop more slowly and are significantly less abundant than cones in zebrafish larvae (Branchek and Bremiller, 1984). Thus, in the original analysis of SynJ1 null zebrafish, we were unsuccessful at identifying mature rod spherules prior to the death of *nrc* mutant fish.

To allow maturation of mutant rods, so that their morphology could be evaluated, we conducted blastula stage transplantation experiments. We transferred cells from SynJ1 null (*nrc*) fish into WT hosts. Thus, transplanted patches of mutant retina can develop within the WT hosts beyond the point at which the *nrc* larvae die. In order to visualize rods, we generated a fish strain containing both the *nrc* mutation and EGFP-positive rods by crossing *nrc* heterozygote zebrafish with the *Tg(xops:EGFP)* zebrafish strain in which EGFP expression is driven specifically in rods by a rhodopsin promoter (Fadool, 2003). Embryos from crosses between *nrc* heterozygotes, which were positive for *Tg(xops:EGFP)*, were used as donors in blastula transplantation experiments. Hosts were WT embryos. To identify the genotypes of the donors used for each transplantation experiment, the donor embryos were grown, genotyped, and/or screened by OKR. All mutant donors lacked an OKR response.

As a control for this experiment, we first established that we could detect morphological abnormalities in mutant fluorescent cones both in a mutant larvae and when transplanted to a WT host. This control experiment was critical for two reasons. First, since the original morphological analysis of *nrc* cones was done with electron microscopy we needed to verify that morphological abnormalities of *nrc* cones could be detected by fluorescence and confocal microscopy. Second, in order to conclude that the normal morphology of mutant rods within the transplants was indicative of the ability of those rods to develop normally, we first needed to establish that mutant cones retained their abnormal morphology in the WT environment. To evaluate cone morphology we used two transgenic strains, *Tg(TalphaC:EGFP)* and *Tg(TalphaC:spH)* expressing EGFP or synapto-pHluorin (respectively) specifically in cones. In the *Tg(TalphaC:EGFP)* cones express EGFP throughout the cell in the cytosol. In contrast, synapto-pHluorin (spH) is a pH-sensitive version of GFP that is tagged to the vesicle protein VAMP-2 (Miesenbock et al., 1998). As a result, in the transgenic strain *Tg(TalphaC:spH)*, spH is concentrated in the cone synapse, but can also be found throughout the cone cell membrane. Since the original analysis of *nrc* occurred at 5 and 6 dpf we analyzed cones both in the transgenic and transplanted fish at this age.

Figure 5A,B shows WT and *nrc* larvae with the transgene *Tg(TalphaC:EGFP)* and Figure 5C,D shows WT and *nrc* larvae expressing the transgene *Tg(TalphaC:spH).* In WT (Fig. 5A,C) sections, the cone pedicle looks like a donut with the dark center showing the invaginations from nonfluorescent secondary cells (arrows). The lack of this invagination can be seen in the synapses of the *nrc* mutant (Fig. 5B,D) in both of these transgenic strains. In addition, the EGFP fluorescence appeared more diffuse throughout the cell in *nrc* compared to WT. Interestingly, for spH expressed in *nrc* cones, we noted an apparent abundance of fluorescence in the inner segment, suggesting a possible accumulation of vesicles in this region (marked with asterisks in 5D). We did not detect this accrual of putative vesicles in WT cones expressing spH. Although the identity of this fluorescence needs to be investigated in more detail, this finding is consistent with our detection of SynJ1 protein in the inner segment (Fig. 2E,F) and supports a possible role for SynJ1 in post-Golgi transport in the photoreceptor inner segment.

To verify that the *nrc* cone synapse develops abnormally within a WT environment we analyzed the morphology of the synapse of *nrc* and WT cones transplanted into WT hosts (Fig. 5E–M). As expected, WT cones expressing either EGFP ($n = 138$) or spH ($n = 63$) retained an invaginated synapse when transplanted into a WT host (Fig. 5E,F,J,K). In

contrast, *nrc* cones appeared *nrc*-like even when in a WT host (Fig. 5G,H,L,M; $n = 20$ for *TalphaC:EGFP* and $n = 16$ for *TalphaC: spH*). An invaginated cone pedicle was not detected in the majority of mutant cones after being transplanted. In addition, other features such as the diffuse EGFP staining and accumulation of fluorescent puncta in the IS in *nrc* cones expressing synapto-pHluorin were also retained after transplantation into a WT host (asterisks in Fig. 5L,M). Quantification of our data is presented in Figure 5I,N. To ensure that we did not bias our analysis of the data, we randomized the images of cones, and rated them for invagination on a three-point scale. Synapses were rated as "invaginated" when they displayed a clearly visible WT-like synaptic invagination and "nrc-like" when no invagination was visible and the overall phenotype resembled cones in the *nrc* mutant. Intermediate phenotypes such as synapses with a possible invagination and distorted morphology were rated as "intermediate." Subsequent to the rating, the cone genotypes were noted and the results were graphed (Fig. 5I,N).

Since we could clearly distinguish fluorescent *nrc* donor cones from WT donor cones in a WT host retina, we proceeded to analyze *nrc* mutant rod morphology using this approach. Transplanted donor-rod photoreceptors were clearly identifiable in the WT host retina because donor fish carried a transgene expressing EGFP under the control of the *Xenopus* opsin promoter. To ensure rod maturation, we allowed the transplanted rods to develop for several weeks in the WT hosts. After 2–3 weeks postfertilization (pf), eyes from hosts containing EGFP-positive transplants were embedded, sectioned, and rod synapses were evaluated by confocal microscopy (Fig. 5P–S). As expected for a successful blastula transplant, EGFP-positive donor rods were sparsely distributed within the WT-host retina and they were correctly localized in the outer retina. We did not detect any differences in transplantation rates, distribution, or localization between transplanted rods from WT donors or *nrc* mutant donors.

In WT retinas the rod spherule has a horseshoe shape. Additionally, an invagination is recognizable at the site of the rod spherule where postsynaptic processes from horizontal cells and bipolar cells contact the terminal. This invagination is clearly defined by EGFP fluorescence in the *Tg(xops:EGFP)* transgenic fish (Fig. 5O). EGFP also uniformly labels the rod cell bodies (Fig. 5O).

Figure 5P–S shows representative WT (5P,Q) and mutant (5R,S) rods in WT hosts. Invaginated synapses appeared at similar frequencies in both WT and *nrc* rod transplants (Fig. 5T). Similar to the cone transplants, we randomized the data, scored the synapse morphology, and then resorted the transplanted rods into groups of *nrc* ($n = 68$) or WT ($n = 58$) donors. The overall rod morphologies of WT and *nrc* transplants were indistinguishable. Both WT rod and *nrc* rod transplants had cell bodies and invaginated, horseshoe-shaped synapses that resembled rod photoreceptors of WT retinas. These findings demonstrate that the morphology of *nrc* mutant rod photoreceptors is not affected by the absence of SynJ1.

## DISCUSSION

This study made two significant findings. First, IHC data demonstrate that SynJ1 is abundant in cone but not rod photoreceptors. Second, rod photoreceptors do not require SynJ1 for proper development, as shown by our blastula transplantation experiments. These findings highlight an important molecular difference between rods and cones. Our findings suggest that SynJ1 contributes to important physiological differences between these cell types.

## Role of SynJ1 in neurons

SynJ1 is a polyphosphoinositide phosphatase that is highly conserved among species (≈80% similar in its functional domains). It exists in two splice forms, 172 kDa and 145 kDa in size. The 172-kDa splice form is expressed in nonneuronal cells in humans, while the shorter 145-kDa splice variant is in neurons (McPherson et al., 1994; Ramjaun and McPherson, 1996). SynJ1 contains three functional domains: two phosphatase domains (Sac1, 5′Ptase) and one proline-rich domain. The Sac1 phosphatase domain can dephosphorylate phosphoinositide (PI) substrates PI(4)P, PI(3)P, and PI(3,5)$P_2$ at several ring positions, while the 5′Ptase domain can remove the phosphate from PI(4,5)$P_2$ and PI(3,4,5)$P_3$ at the 5′-position only (Guo et al., 1999). The proline-rich domain offers binding sites for proteins with SH3 domains such as amphiphysin and endophilin (McPherson et al., 1996; Haffner et al., 1997, 2000; Nemoto et al., 1997; Ringstad et al., 1997).

Phosphoinositide metabolism plays a significant role in synapse function, as phosphoinositides are thought to be key regulators of the vesicle cycle as well as actin cytoskeleton organization (Cremona and De Camilli, 1997). For example, PI(4,5)$P_2$ promotes actin nucleation and also clathrin coating of vesicles, which is essential for endocytosis (Cremona and De Camilli, 2001). Since SynJ1 regulates phosphoinositide metabolism, SynJ1 deficiency has dramatic consequences, especially in neurons where synaptic vesicles must be constantly recycled. Vesicles in SynJ1-deficient neurons frequently line up abnormally in a row or form vesicle clusters. Vesicles also fail to shed clathrin-coats or participate in the vesicle cycle (Cremona et al., 1999; Guo et al., 1999; Harris et al., 2000; Stefan et al., 2002, 2005; Verstreken et al., 2003). These phenotypes, which are very consistent among different species, illustrate the importance of SynJ1 (Cremona et al., 1999; Guo et al., 1999; Harris et al., 2000; Stefan et al., 2002, 2005; Verstreken et al., 2003).

## SynJ1 has an important function in cone, but not rod photoreceptor synapses

Recent studies conducted in our laboratory have extended the role of SynJ1 from conventional synapses to ribbon synapses (Van Epps et al., 2004). We previously determined that the zebrafish mutant *nrc* lacks SynJ1. This mutant has a number of phenotypes in addition to the SynJ1-deficient phenotypes known from conventional synapses (Allwardt et al., 2001; Van Epps et al., 2004). Namely, in the zebrafish *nrc* mutant, ribbon structures in cone synapses are formed, but unanchored due to the absence of the arciform density, which usually anchors ribbon structures to the plasma membrane. Synaptic vesicles are present, but in lower number. The vesicles also form aggregates and are unevenly dispersed, which is consistent with the morphological changes associated with SynJ1 deficiency in conventional neurons. Overall, this leads to defective synaptic transmission between cones and secondary retinal neurons causing blindness in *nrc* mutants (Allwardt et al., 2001; Van Epps et al., 2001).

SynJ1 deficiency affects ribbons in cones, but not bipolar cells (Allwardt et al., 2001). This finding suggests that cones have a unique requirement for SynJ1 and phosphoinositides. Another formal possibility was that a gene duplication or splice variant of SynJ1 functions in bipolar cells and complements the *nrc* mutation. Several lines of evidence rule out this latter possibility. First, no additional copies of the SynJ1 gene have been identified by searches of the zebrafish genome database. Second, antibodies against both zebrafish and rat synaptojanin 1 do not detect additional immunoreactive species in *nrc* mutants (Fig. 1B,C in this study, and Van Epps et al., 2004). Third, the *nrc* mutation introduces a stop codon at the end of the SAC domain. This prevents formation of both known splice forms of SynJ1 because this exon is predicted to be in both the 145- and 172-kDa forms (Ramjaun and McPherson, 1996; Van Epps et al., 2004).

Given the apparent special requirement of cone ribbon versus bipolar ribbon synapses for SynJ1, we asked whether rods require SynJ1 for proper development. This question was difficult to address in the initial studies characterizing the *nrc* mutation due to premature death of *nrc* mutants. In zebrafish larvae, rods are much less abundant than cones: rods appear and mature in the retina over a protracted time frame (Branchek, 1984; Branchek and Bremiller, 1984; Raymond et al., 1995). To address this question, we developed a monoclonal antibody that specifically recognizes zebrafish SynJ1 (Fig. 1). While cone pedicles were clearly labeled in the adult zebrafish retina by our zfSynJ1 antibody (Fig. 3), we failed to detect significant SynJ1 in rod spherules (Fig. 4), suggesting that SynJ1 is present only in low levels or entirely absent in rod terminals. This finding was rather surprising, as rod and cone photoreceptor synapses face similar synaptic transmission challenges (discussed below). In an independent approach we used blastula transplantation experiments to verify that rods do not require SynJ1. After performing blastula transplantations, we analyzed the development of EGFP-labeled *nrc* mutant rod photoreceptors in a WT fish that was capable of growing to adulthood. Rods were allowed to mature for ≈3 weeks pf before we analyzed the *nrc* mutant rod spherules. The EGFP expression allowed us to identify mutant rods in WT hosts. Using this approach we showed that *nrc* mutant rod spherules form normally and display no apparent morphological defects (Fig. 5). Control experiments with transplanted *nrc* cones demonstrated that the WT host retinal environment could not rescue the *nrc* cone morphological defects. Altogether, our findings show that SynJ1 is significantly less abundant in rod photoreceptors than in cones and that the *nrc* mutant phenotype is limited to cone pedicles.

## Differences and similarities between rod and cone synapses

Rod and cone photoreceptors are specialized neurons designed to detect light. They use similar, but not identical phototransduction cascades. They are depolarized in darkness and are hyperpolarized by light (Chen, 2005). In darkness rods and cones release glutamate by synaptic vesicle fusion. Light-induced hyperpolarization slows the release of vesicles (Heidelberger, 2007). This poses special challenges for rod and cone synapses. To meet these challenges both rod and cones use ribbon synapses that facilitate tonic and graded neurotransmitter release (Parsons and Sterling, 2003; Sterling and Matthews, 2005).

Despite facing similar functional challenges, there are obvious anatomical differences between rod spherules and cone pedicles (for review, see Sterling and Matthews, 2005). Within species, rod spherules are generally significantly smaller than cone pedicles. Additionally, the postsynaptic processes from bipolar and horizontal cells are aligned differently in rod and cone synapses (Rao-Mirotznik et al., 1995; Haverkamp et al., 2000). Another striking difference between cone and rod synapses is that cone pedicles contain multiple ribbon structures attached to multiple active zones, whereas rod spherules contain a single ribbon structure. Consequently, cone pedicles can provide a larger number of docking sites, possess a larger vesicle pool than rod spherules, and have a higher information transmission rate.

Rod/cone differences are not limited to morphology; they also extend to the molecular level. There is evidence that rod and cone synapses express different L-type Ca channel subtypes (Morgans, 1999; Firth et al., 2001; Morgans, 2001). Rod and cone synapses also express different isoforms of the synaptic vesicle protein SV2, a calcium-sensing protein. Rod spherules only contain the SV2B isoform, whereas cone pedicles possess the SV2A and the SV2B isoform (Wang et al., 2003). Adding to the list of molecular differences between rod and cone synapses, we have now presented evidence that SynJ1 is expressed predominately in cone pedicles, but not in rod spherules, and that SynJ1 deficiency in *nrc* mutant zebrafish affects only cone ribbon synapse morphology. Therefore rods, unlike cones, are able to develop and perform their normal physiological functions without SynJ1 activity.

The high transmission rate of cones means that they replenish their vesicle pool by a high endocytosis rate. SynJ1 plays an important role in endocytosis. Studies examining endocytosis at cones and bipolar ribbons clearly demonstrate that different ribbon-type synapses employ unique endocytic strategies. While cones endocytose their membrane as small vesicles (Rea et al., 2004), retinal bipolar cells use bulk endocytosis into large endosomes (Holt et al., 2003; Paillart et al., 2003). Our findings suggest differences in endocytosis between rod spherules and cone pedicles as well. The lack of obvious morphological defects in *nrc* rods as well as the reduced SynJ1 immunoreactivity in rods compared to cones suggests that rod spherules and cone pedicles have evolved different ways to either regulate endocytosis and/or replenish endocytic vesicle pools. Further studies examining SynJ1 function in cones are needed to explain the biochemical basis for the differences between rod spherules and cone pedicles. Future studies will also address whether a different phosphoinositide phosphatase, such as Synaptojanin 2, is important for rod synapse function.

## Supplementary Material

Refer to Web version on PubMed Central for supplementary material.

## Acknowledgments

Grant sponsor: National Institutes of Health (NIH); Grant numbers: RO1EY01565 (to S.E.B.), P30EY01730 (to UW Vision Core Facility), T32EY007031 (to A.A.L.).

We thank Daniel Possin for assistance with imaging, Jing Huang for monoclonal antibody production, Ken Lindsay for help with tissue culture, Huy Nguyen for help with graphics, Professor James B. Hurley for comments on the article and Rachel O. Wong for use of her microscopes.

## LITERATURE CITED

Allwardt BA, Lall AB, Brockerhoff SE, Dowling JE. Synapse formation is arrested in retinal photoreceptors of the zebrafish nrc mutant. J Neurosci. 2001; 21:2330–2342. [PubMed: 11264308]

Arshavsky V. Like night and day: rods and cones have different pigment regeneration pathways. Neuron. 2002; 36:1–3. [PubMed: 12367498]

Branchek T. The development of photoreceptors in the zebrafish, Brachydanio rerio. II. Function. J Comp Neurol. 1984; 224:116–122. [PubMed: 6715575]

Branchek T, Bremiller R. The development of photoreceptors in the zebrafish, Brachydanio rerio. I. Structure. J Comp Neurol. 1984; 224:107–115. [PubMed: 6715574]

Brockerhoff SE. Measuring the optokinetic response of zebrafish larvae. Nat Protoc. 2006; 1:2448–2451. [PubMed: 17406490]

Brockerhoff SE, Hurley JB, Niemi GA, Dowling JE. A new form of inherited red-blindness identified in zebrafish. J Neurosci. 1997; 20:1–8.

Brockerhoff SE, Rieke F, Matthews HR, Taylor MR, Kennedy B, Ankoudinova I, Niemi GA, Tucker CL, Xiao M, Cilluffo MC, Fain GL, Hurley JB. Light stimulates a transducin-independent increase of cytoplasmic Ca2+ and suppression of current in cones from the zebrafish mutant nof. J Neurosci. 2003; 23:470–480. [PubMed: 12533607]

Carmany-Rampey A, Moens CB. Modern mosaic analysis in the zebrafish. Methods. 2006; 39:228–238. [PubMed: 16829130]

Chen CK. The vertebrate phototransduction cascade: amplification and termination mechanisms. Rev Physiol Biochem Pharmacol. 2005; 154:101–121. [PubMed: 16634148]

Cremona O, De Camilli P. Synaptic vesicle endocytosis. Curr Opin Neurobiol. 1997; 7:323–330. [PubMed: 9232811]

Cremona O, De Camilli P. Phosphoinositides in membrane traffic at the synapse. J Cell Sci. 2001; 114(Pt 6):1041–1052. [PubMed: 11228149]

Cremona O, Di Paolo G, Wenk MR, Luthi A, Kim WT, Takei K, Daniell L, Nemoto Y, Shears SB, Flavell RA, McCormick DA, De Camilli P. Essential role of phosphoinositide metabolism in synaptic vesicle recycling. Cell. 1999; 99:179–188. [PubMed: 10535736]

Fadool JM. Development of a rod photoreceptor mosaic revealed in transgenic zebrafish. Dev Biol. 2003; 258:277–290. [PubMed: 12798288]

Firth SI, Morgan IG, Boelen MK, Morgans CW. Localization of voltage-sensitive L-type calcium channels in the chicken retina. Clin Exp Ophthalmol. 2001; 29:183–187.

Fu Y, Yau KW. Phototransduction in mouse rods and cones. Pflugers Arch. 2007; 454:805–819. [PubMed: 17226052]

Guo S, Stolz LE, Lemrow SM, York JD. SAC1-like domains of yeast SAC1, INP52, and INP53 and of human synaptojanin encode polyphosphoinositide phosphatases. J Biol Chem. 1999; 274:12990–12995. [PubMed: 10224048]

Haffner C, Takei K, Chen H, Ringstad N, Hudson A, Butler MH, Salcini AE, Di Fiore PP, De Camilli P. Synaptojanin 1: localization on coated endocytic intermediates in nerve terminals and interaction of its 170 kDa isoform with Eps15. FEBS Lett. 1997; 419:175–180. [PubMed: 9428629]

Haffner C, Di Paolo G, Rosenthal JA, de Camilli P. Direct interaction of the 170 kDa isoform of synaptojanin 1 with clathrin and with the clathrin adaptor AP-2. Curr Biol. 2000; 10:471–474. [PubMed: 10801423]

Harris TW, Hartwieg E, Horvitz HR, Jorgensen EM. Mutations in synaptojanin disrupt synaptic vesicle recycling. J Cell Biol. 2000; 150:589–600. [PubMed: 10931870]

Haverkamp S, Grunert U, Wassle H. The cone pedicle, a complex synapse in the retina. Neuron. 2000; 27:85–95. [PubMed: 10939333]

Heidelberger R. Mechanisms of tonic, graded release: lessons from the vertebrate photoreceptor. J Physiol. 2007; 585(Pt 3):663–667. [PubMed: 17584835]

Holt M, Cooke A, Wu MM, Lagnado L. Bulk membrane retrieval in the synaptic terminal of retinal bipolar cells. J Neurosci. 2003; 23:1329–1339. [PubMed: 12598621]

Joselevitch C, Klooster J, Kamermans M. Localization of metabotropic glutamate receptors in the outer plexiform layer of the goldfish retina. Cell Tissue Res. 2007; 330:389–403. [PubMed: 17906878]

Kawamura S, Tachibanaki S. Rod and cone photoreceptors: molecular basis of the difference in their physiology. Comp Biochem Physiol A Mol Integr Physiol. 2008; 150:369–377. [PubMed: 18514002]

Kennedy BN, Alvarez Y, Brockerhoff SE, Stearns GW, Sapetto-Rebow B, Taylor MR, Hurley JB. Identification of a zebrafish cone photoreceptor-specific promoter and genetic rescue of achromatopsia in the nof mutant. Invest Ophthalmol Vis Sci. 2007; 48:522–529. [PubMed: 17251445]

Korenbrot JI, Rebrik TI. Tuning outer segment Ca2+ homeostasis to phototransduction in rods and cones. Adv Exp Med Biol. 2002; 514:179–203. [PubMed: 12596922]

Mata NL, Radu RA, Clemmons RC, Travis GH. Isomerization and oxidation of vitamin a in cone-dominant retinas: a novel pathway for visual-pigment regeneration in daylight. Neuron. 2002; 36:69–80. [PubMed: 12367507]

Mata NL, Ruiz A, Radu RA, Bui TV, Travis GH. Chicken retinas contain a retinoid isomerase activity that catalyzes the direct conversion of all-trans-retinol to 11-cis-retinol. Biochemistry. 2005; 44:11715–11721. [PubMed: 16128572]

McPherson PS, Takei K, Schmid SL, De Camilli P. p145, a major Grb2-binding protein in brain, is co-localized with dynamin in nerve terminals where it undergoes activity-dependent dephosphorylation. J Biol Chem. 1994; 269:30132–30139. [PubMed: 7982917]

McPherson PS, Garcia EP, Slepnev VI, David C, Zhang X, Grabs D, Sossin WS, Bauerfeind R, Nemoto Y, De Camilli P. A presynaptic inositol-5-phosphatase. Nature. 1996; 379:353–357. [PubMed: 8552192]

Miesenbock G, De Angelis DA, Rothman JE. Visualizing secretion and synaptic transmission with pH-sensitive green fluorescent proteins. Nature. 1998; 394:192–195. [PubMed: 9671304]

Morgans CW. Calcium channel heterogeneity among cone photo-receptors in the tree shrew retina. Eur J Neurosci. 1999; 11:2989–2993. [PubMed: 10457194]

Morgans CW. Localization of the alpha(1F) calcium channel subunit in the rat retina. Invest Ophthalmol Vis Sci. 2001; 42:2414–2418. [PubMed: 11527958]

Muto A, Orger MB, Wehman AM, Smear MC, Kay JN, Page-McCaw PS, Gahtan E, Xiao T, Nevin LM, Gosse NJ, Staub W, Finger-Baier K, Baier H. Forward genetic analysis of visual behavior in zebrafish. PLoS Genet. 2005; 1:e66. [PubMed: 16311625]

Nemoto Y, Arribas M, Haffner C, DeCamilli P. Synaptojanin 2, a novel synaptojanin isoform with a distinct targeting domain and expression pattern. J Biol Chem. 1997; 272:30817–30821. [PubMed: 9388224]

Paillart C, Li J, Matthews G, Sterling P. Endocytosis and vesicle recycling at a ribbon synapse. J Neurosci. 2003; 23:4092–4099. [PubMed: 12764096]

Parsons TD, Sterling P. Synaptic ribbon. Conveyor belt or safety belt? Neuron. 2003; 37:379–382. [PubMed: 12575947]

Ramjaun AR, McPherson PS. Tissue-specific alternative splicing generates two synaptojanin isoforms with differential membrane binding properties. J Biol Chem. 1996; 271:24856–24861. [PubMed: 8798761]

Rao-Mirotznik R, Harkins AB, Buchsbaum G, Sterling P. Mammalian rod terminal: architecture of a binary synapse. Neuron. 1995; 14:561–569. [PubMed: 7695902]

Raymond PA, Barthel LK, Curran GA. Developmental patterning of rod and cone photoreceptors in embryonic zebrafish. J Comp Neurol. 1995; 359:537–550. [PubMed: 7499546]

Rea R, Li J, Dharia A, Levitan ES, Sterling P, Kramer RH. Streamlined synaptic vesicle cycle in cone photoreceptor terminals. Neuron. 2004; 41:755–766. [PubMed: 15003175]

Ringstad N, Nemoto Y, De Camilli P. The SH3p4/Sh3p8/SH3p13 protein family: binding partners for synaptojanin and dynamin via a Grb2-like Src homology 3 domain. Proc Natl Acad Sci U S A. 1997; 94:8569–8574. [PubMed: 9238017]

Schroeter EH, Wong RO, Gregg RG. In vivo development of retinal ON-bipolar cell axonal terminals visualized in nyx::MYFP transgenic zebrafish. Vis Neurosci. 2006; 23:833–843. [PubMed: 17020638]

Stearns G, Evangelista M, Fadool JM, Brockerhoff SE. A mutation in the cone-specific pde6 gene causes rapid cone photoreceptor degeneration in zebrafish. J Neurosci. 2007; 27:13866–13874. [PubMed: 18077698]

Stefan CJ, Audhya A, Emr SD. The yeast synaptojanin-like proteins control the cellular distribution of phosphatidylinositol (4,5)-bisphosphate. Mol Biol Cell. 2002; 13:542–557. [PubMed: 11854411]

Stefan CJ, Padilla SM, Audhya A, Emr SD. The phosphoinositide phosphatase Sjl2 is recruited to cortical actin patches in the control of vesicle formation and fission during endocytosis. Mol Cell Biol. 2005; 25:2910–2923. [PubMed: 15798181]

Sterling P, Matthews G. Structure and function of ribbon synapses. Trends Neurosci. 2005; 28:20–29. [PubMed: 15626493]

Taylor MR, Kikkawa S, Diez-Juan A, Ramamurthy V, Kawakami K, Carmeliet P, Brockerhoff SE. The zebrafish pob gene encodes a novel protein required for survival of red cone photoreceptor cells. Genetics. 2005; 170:263–273. [PubMed: 15716502]

Thoreson WB. Kinetics of synaptic transmission at ribbon synapses of rods and cones. Mol Neurobiol. 2007; 36:205–223. [PubMed: 17955196]

Van Epps HA, Yim CM, Hurley JB, Brockerhoff SE. Investigations of photoreceptor synaptic transmission and light adaptation in the zebrafish visual mutant nrc. Invest Ophthalmol Vis Sci. 2001; 42:868–874. [PubMed: 11222552]

Van Epps HA, Hayashi M, Lucast L, Stearns GW, Hurley JB, De Camilli P, Brockerhoff SE. The zebrafish nrc mutant reveals a role for the polyphosphoinositide phosphatase synaptojanin 1 in cone photoreceptor ribbon anchoring. J Neurosci. 2004; 24:8641–8650. [PubMed: 15470129]

Verstreken P, Koh TW, Schulze KL, Zhai RG, Hiesinger PR, Zhou Y, Mehta SQ, Cao Y, Roos J, Bellen HJ. Synaptojanin is recruited by endophilin to promote synaptic vesicle uncoating. Neuron. 2003; 40:733–748. [PubMed: 14622578]

Wang MM, Janz R, Belizaire R, Frishman LJ, Sherry DM. Differential distribution and developmental expression of synaptic vesicle protein 2 isoforms in the mouse retina. J Comp Neurol. 2003; 460:106–122. [PubMed: 12687700]

Westerfield, M. The zebrafish book: a guide for the laboratory use of zebrafish (Brachydanio rerio). Eugene: University of Oregon Press; 1995.

Yazulla S, Studholme KM. Neurochemical anatomy of the zebrafish retina as determined by immunocytochemistry. J Neurocytol. 2001; 30:551–592. [PubMed: 12118162]

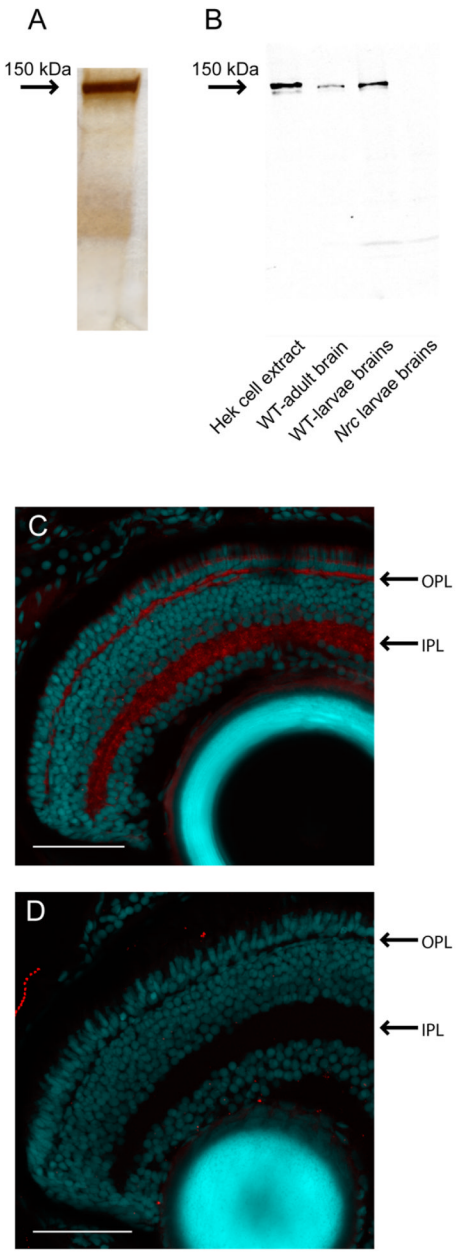


**Figure 1.**

SynJ1 antibody is highly specific. **A:** Silver stain-PAGE of purified His-tagged SynJ1. **B:** Western blot analysis with anti-zfSynJ1 antibody. **C,D:** Larval retinal sections (dpf6) from WT (C) and *nrc* mutant zebrafish (D) labeled with the anti-zfSynJ1 antibody (red) and propidium iodide nuclear stain (cyan). OPL, outer plexiform layer; IPL, inner plexiform layer. Scale bars = 100 $\mu$m.

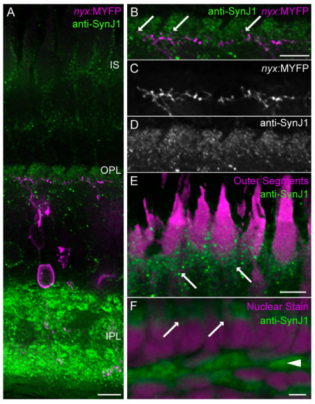


**Figure 2.**

SynJ1 is localized to photoreceptor terminals and inner segments. **A:** Adult zebrafish retinal section from the transgenic zebrafish line *Tg(nyx:MYFP)* immunolabeled for SynJ1 (green). YFP expressing ON-bipolar cells are pseudocolored magenta. B–D: Magnified OPL from the region shown in (A). **B:** The merged imaged. Synaptic invaginations are marked with arrows. **C:** The YFP-labeled bipolar dendrites. **D:** SynJ1 alone. **E:** Magnified inner segment from region shown in (A). Autofluorescing outer segments are pseudocolored magenta, inner segments are marked with arrows. **F:** High-power view of a WT larval retinal section labeled with anti-zf-SynJ1 antibody (green) and propidium iodide nuclear stain (magenta). OPL is marked with an arrowhead and the inner segment region is marked with arrows. Scale bars = 5 $\mu$m for all panels.

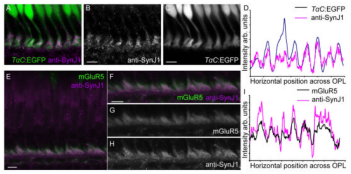


**Figure 3.**

SynJ1 is present in cone pedicles. A–C: Adult zebrafish retinal section from the transgenic zebrafish line *Tg(TalphaC:EGFP)* immunolabeled for SynJ1. The SynJ1 staining colocalizes with the EGFP signal in cone photoreceptors. **A:** merged image of *Tg(TalphaC:EGFP)* (green) and anti-SynJ1 (magenta). **B:** Anti-SynJ1 alone. **C:** *Tg(TalphaC:EGFP)* alone. **D:** Overlaid intensity profiles of the cone-EGFP and anti-zf-SynJ1 label in the OPL region of the image shown in (A). The similarity of the peak locations supports the colocalization of these markers (please see Materials and Methods for a description of how these graphs were created). **E:** Merged image of a WT adult retinal section immunolabeled with anti-zfSynJ1 and anti-mGluR5 antibodies. F–H: Magnified image of the OPL region from (E) showing colocalization. **F:** Merged image of anti-mGluR5 (green) and anti-SynJ1(magenta). **G:** Anti-mGluR5 alone. **H:** Anti-zfSynJ1 alone. **I:** Overlaid intensity profiles of SynJ1 and mGluR5 fluorescence within the OPL. Scale bars = 5 $\mu$m for all panels.

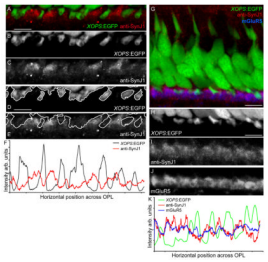

**Figure 4.**

SynJ1 is more abundant in cones pedicles than in rod spherules. Adult retinal sections from the transgenic *Tg(xops:EGFP)* zebrafish immunolabeled for zfSynJ1 alone (A–F) or zfSynJ1 and mGluR5 together (G–K). **A:** The OPL region showing *xops*:EGFP expression (green) and anti-SynJ1 labeling (red). Strongest SynJ1-label appears outside of EGFP-labeled rod terminals. **B:** The EGFP-labeled rod spherules alone. **C:** Anti-SynJ1 alone. **D:** The EGFP labeled rod spherules (B) were outlined. **E:** Outlined rod spherules superimposed onto an image displaying the SynJ1 label. **F:** Overlaid intensity profiles of *xops:*EGFP and SynJ1 label showing the dissimilarity in the location of the peak signals. **G:** The triple label of *xops*::EGFP (green), anti-zfSynJ1 (red), and mGluR5 (blue). **H:** *xops*:EGFP alone. **I:** Anti-zfSynJ1 alone. **J:** mGluR5 alone. **K:** Overlaid intensity profiles of *xops:*EGFP, anti-zfSynJ1, and mGluR5 showing the convergence of the SynJ1 and mGlu5 signals and the divergence of the EGFP peaks. Scale bars = 5 $\mu$m for all panels.

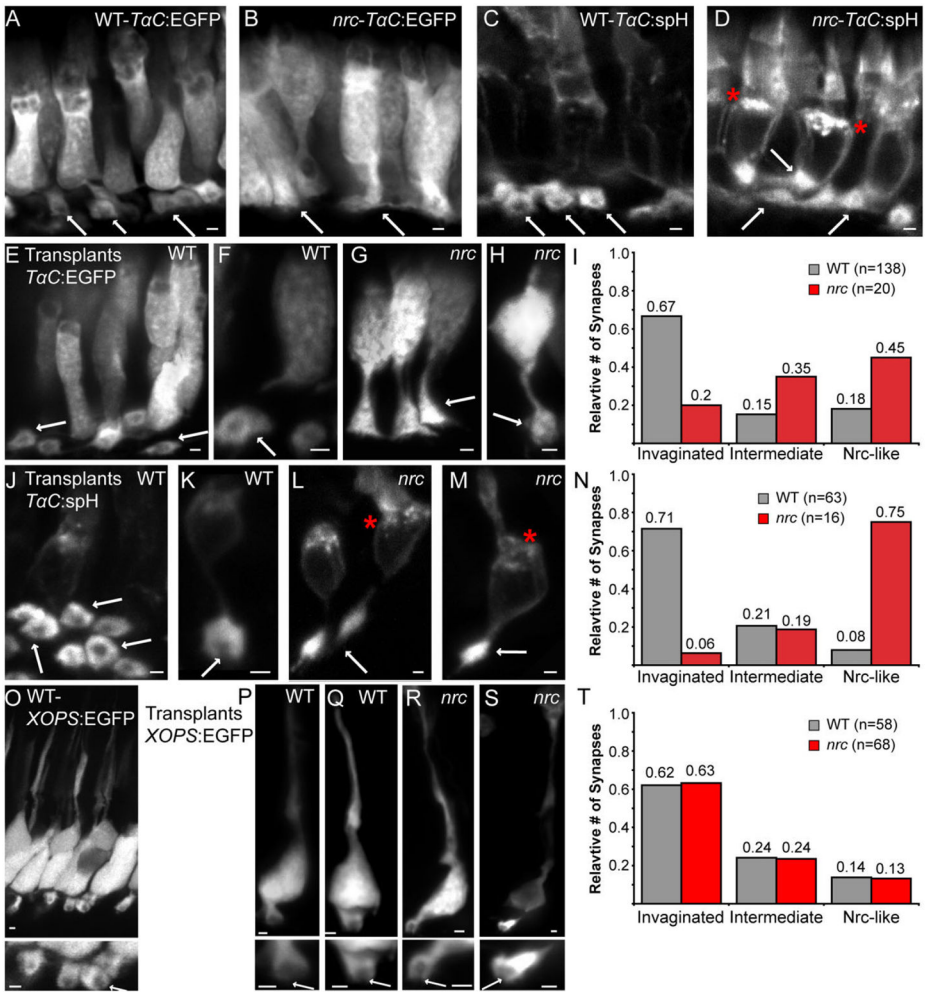


**Figure 5.**

Transplanted *nrc* mutant rod terminals appear normal. **A,B:** Confocal images of retinal sections from WT (A) and *nrc* mutant (B) larvae (dpf6) containing transgene *Tg(TalphaC:EGFP)*. **C,D:** Retinal sections from WT (C) and *nrc* mutant (D) zebrafish larvae (dpf6) carrying the transgene *Tg(TalphaC:spH)*. For all images, asterisks demark an accumulation of fluorescence in the inner segments of *nrc* mutant cones. Arrows point to cone synaptic terminals. **E–M:** Cells from WT and *nrc* fish containing either *Tg(TalphaC:EGFP)* (E–H) or *Tg(TalphaC:spH)* (J–M) were transplanted into a WT host (see Materials and Methods). Please note, for transplanted cones we refer to both genotypic het and WT cones as WT since no ultrastructural abnormalities have been noted in cones from *nrc* heterozygotes. At 6 dpf, fish were sectioned and transplanted cones were identified by fluorescence. Asterisks (L,M) mark an abundance of putative vesicles in *nrc* cone transplants from the *Tg(TalphaC:spH)* fish line. **I,N:** Synapses of transplanted WT and *nrc* mutant cone terminals were placed into categories; “Invaginated” with a WT appearing synaptic invagination, “intermediate,” with a possible invagination, and “nrc-like” with no obvious synaptic invagination (see Results). A greater percentage of the transplanted *nrc* mutant cone synapses ($n = 20$ [EGFP]; $n = 16$ [spH]) lack invaginations compared to transplanted WT cone synapses ($n = 138$ [EGFP]; $n = 68$ [spH]). Two-tailed *P*-values for cone transplants are (I) $6 \times 10^{-4}$ (*TalphaC:EGFP*) and (N) $5.3 \times 10^{-8}$ (*TalphaC:spH*). **O:** Confocal micrograph of a WT adult retinal section from *Tg(xops:EGFP)* zebrafish showing

synaptic invaginations into rod spherules. **P–S:** Cells from WT (P,Q) and *nrc* (R,S) fish containing *Tg(xops:EGFP)* were transplanted into a WT host. After 2–3 weeks pf fish were sectioned and transplanted rods were identified by fluorescence. Higher-magnification pictures of the terminals are provided in the respective bottom panels. Synaptic invaginations are marked by arrows. **T:** The synapse and cell morphology of transplanted WT and *nrc* mutant rod terminals were scored and no differences were observed. Scale bars = 1 $\mu$m for all panels.

## TABLE 1

List of Primary Antibodies

| Antigen | Immunogen | Host | Source | Dilution |
|---|---|---|---|---|
| SynJ1 | Full-length zf-SynJ1 (His-tagged) *accession number: NP_001007031* | Mouse IgG, monoclonal | Monoclonal hybridoma cell culture | 1:5 (Immunoblot), undiluted (IHC) |
| mGluR5 | Synthetic peptide from rat mGluR5 Seq: CIP-SSP-KYD-TLI-IRD-YTQ-SSS-SL | Rabbit IgG, polyclonal | Chemicon International, #AB5675 | 1:750 (IHC) |
| His tag | Synthetic peptide of 6X His | Mouse, IgG monoclonal | Invitrogen, #37-2900 | 1:1,000 (Immunoblot) |